ACS APPLIED MATERIALS & INTERFACES

Research Article

www.acsami.org

Stable and High-Performance Flexible ZnO Thin-Film Transistors by Atomic Layer Deposition

Yuan-Yu Lin,[†] Che-Chen Hsu,[†] Ming-Hung Tseng,[†] Jing-Jong Shyue,[†,‡] and Feng-Yu Tsai*[,†]

[†]Department of Materials Science and Engineering, National Taiwan University, 1, Section 4, Roosevelt Road, Taipei 106, Taiwan, R.O.C.

[‡]Research Center for Applied Science, Academia Sinica, Taipei 115, Taiwan, R. O. C.

Supporting Information

ABSTRACT: Passivation is a challenging issue for the oxide thin-film transistor (TFT) technologies because it requires prolonged high-temperature annealing treatments to remedy defects produced in the process, which greatly limits its manufacturability as well as its compatibility with temperature-sensitive materials such as flexible plastic substrates. This study investigates the defect-formation mechanisms incurred by atomic layer deposition (ALD) passivation processes on ZnO TFTs, based on which we demonstrate for the first time degradation-free passivation of ZnO TFTs by a TiO_2/Al_2O_3 nanolaminated (TAO) film deposited by a low-temperature (110 °C) ALD process. By combining the TAO passivation film with ALD dielectric and channel layers into an integrated low-temperature ALD process, we successfully fabricate flexible ZnO TFTs on plastics. Thanks to the exceptional gas-barrier property of the TAO film (water vapor transmission rate (WVTR) < 10^{-6} g m^{-2} day^{-1}) as well as the defect-free nature of the ALD dielectric and ZnO channel layers, the TFTs exhibit excellent device performance with high stability and flexibility: field-effect mobility >20 cm^2 V^{-1} s^{-1}, subthreshold swing < 0.4 V $decade^{-1}$ after extended bias-stressing (>10 000 s), air-storage (>1200 h), and bending (1.3 cm radius for 1000 times).

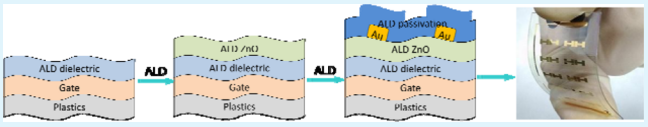

KEYWORDS: *atomic layer deposition, thin film transistors, passivation, flexible electronics, gas barrier*

1. INTRODUCTION

Metal-oxide-based thin film transistors (TFTs) offer many advantages over silicon-based TFTs, including low processing temperature, high carrier mobility, optical transparency, and ease of production, and therefore are heralded as the primary alternative TFT technology.[1] But unlike silicon, whose stable and insulating oxide can protect it against environment-induced degradations, the oxide semiconductor in a TFT must be passivated with an overcoated barrier layer to shield against damages that may be incurred by the TFT's subsequent processing and use.[2−6] Deposition of such a passivation layer, however, inevitably degrades the characteristics of the oxide semiconductor due to the defect-inducing interactions between the oxide semiconductor and the passivation processing environment.[7] As a result, an extended high-temperature postpassivation annealing step is required to remedy the defects created during the passivation process and to reverse the degradations.[8] Such an annealing step not only greatly increases the production time and cost of oxide TFTs, but is incompatible with temperature-sensitive device materials such as flexible plastic substrates, preventing oxide TFT applications in flexible and organic electronics. Consequently, a low-temperature passivation process that does not induce degradations on its passivated TFTs will be highly valuable in the development of the oxide TFT technologies.

In this study, we utilize the technique of atomic layer deposition (ALD) to develop a low-temperature, degradation-free passivation process for flexible ZnO TFTs. ALD is capable of producing defect-free films with exceptional gas-barrier performance at low deposition temperatures,[9−11] and has been widely used for passivating or encapsulating many different types of sensitive electronic devices.[12−20] Moreover, ALD is especially advantageous in terms of manufacturability for flexible electronics applications, thanks to its demonstrated ability to be adapted into large-area, atmospheric roll-to-roll manufacturing processes for flexible electronics.[21−28] For the passivation of oxide TFTs, ALD provides additional benefits in that the dielectric, channel, and passivation layers can all be deposited in an integrated ALD process, which minimizes defect formation at the interfaces and reduces process complexity.[29−37] Previous attempts at utilizing ALD as a passivation method for oxide TFTs, however, have shown that similar to other passivation techniques, ALD passivation also caused severe degradations to oxide TFTs,[8] and therefore successful low-temperature ALD passivation of oxide TFTs has not been demonstrated. To address this issue, we study the mechanism of ALD-passivation-induced degradation to ZnO TFTs by examining various ALD chemistries and processing conditions of several metal oxides that are commonly used as passivation materials, including Al_2O_3, HfO_2, ZrO_2, TiO_2, and their nanolaminates. These metal oxides are popular passivation materials owing to their insulating property, mechanical

Received: August 7, 2015
Accepted: September 25, 2015
Published: October 5, 2015

DOI: 10.1021/acsami.5b07278
ACS Appl. Mater. Interfaces 2015, 7, 22610−22617

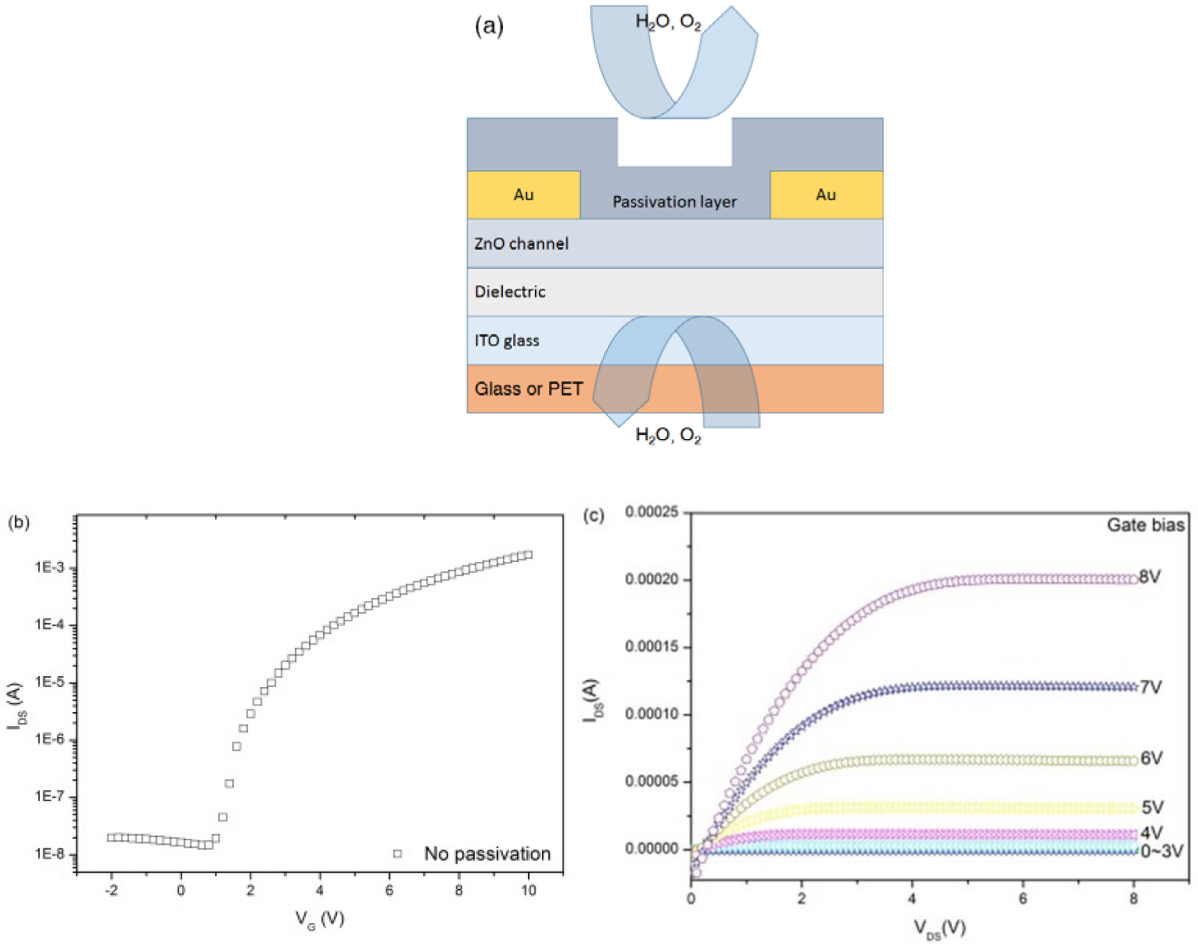

Figure 1. (a) Illustration of the device structure used in this study; (b) transfer and (c) output characteristics of the ZnO TFTs without passivation.

Table 1. Processing Conditions of the ALD Dielectric, Channel, and Passivation Layers Used in the Fabrication of the TFT Devices

film	precursor	pulse time (s)	soaking time (s)	pumping time (s)	cycles/thickness
ZnO	DeZn	0.06	0	30	250/45 nm
	H_2O	0.02	0	30	
Al_2O_3	TMA	0.03	0	8	350/35 nm
	H_2O	0.02	0	8	
HfO_2	TDMAHf	0.1	0	20	350/35 nm
	H_2O	0.02	0	20	
ZrO_2	TDMAZr	0.1	0	20	350/35 nm
	H_2O	0.02	0	20	
TiO_2 from TDMATi	TDMATi	0.1	0	20	875/35 nm
	H_2O	0.02	0	20	
TiO_2 from TTIP	TTIP	0.1	0	20	2333/35 nm
	H_2O	0.02	0	20	
AHO	as dielectric: alternating 20 cycles of Al_2O_3 with 30 cycles of HfO_2 for 8 times as passivation: alternating 20 cycles of Al_2O_3 with 30 cycles of HfO_2 for 7 times				
ATO	alternating 20 cycles of Al_2O_3 with 200 cycles of TiO_2 from TTIP for 7 times				

strength, chemical stability, and optical transparency.[38] ZnO TFTs are used as the platform of this study because ZnO is more prone to environment- and passivation-induced degradation than other oxide semiconductors,[39] and therefore passivation processes identified to be compatible with ZnO TFTs should be readily extendable to other types of oxide TFTs. By understanding the mechanism of passivation-induced degradations, we design and demonstrate for the first time an ALD passivation process that yields degradation-free ZnO TFTs after passivation. We then combine the ALD passivation film with an ALD dielectric and ZnO channel layers into an integrated, low-temperature (≤110 °C) ALD process to fabricate flexible ZnO TFTs on plastic substrates, taking

DOI: 10.1021/acsami.5b07278
ACS Appl. Mater. Interfaces 2015, 7, 22610−22617

advantages of the exceptional quality of the ALD layers to realize unprecedented device performance and stability.

2. EXPERIMENTAL SECTION

2.1. Device Fabrication. The ZnO TFTs analyzed in this study were of a bottom-gate/top-contact device structure, whose schematic illustration is shown in Figure 1. The devices were fabricated on two types of substrates: ITO-coated glass (Rite Displays; sheet resistance = 15 Ω sq^{-1}) for rigid devices and ITO-coated poly(ethyleneterephthalate) (PET) (Perm Top Corp.; sheet resistance = 60 Ω sq^{-1}) for flexible devices. The fabrication procedure was as follows: (1) ITO was patterned into gate electrodes by photolithography followed by wet etching in hydrochloric acid; (2) patterned substrates were cleaned in turn with ultrasonication in acetone, methanol, and deionized water for 10 min, and then cleaned with air plasma (Harrick Scientific, model PDC-32G) for 5 min; (3) a dielectric layer, an alternating Al_2O_3(2 nm)/HfO_2(3 nm) nanolaminated (AHO) film (40 nm of total thickness), was deposited by atomic layer deposition (ALD); (4) after the deposition of the dielectric layer, a 45 nm ZnO channel layer was immediately deposited by ALD without breaking vacuum; (5) source and drain electrodes were formed by thermally evaporating Au (thickness = 100 nm) under high vacuum (10^6 Torr) through a shadow mask; the channel length/width (L/W) were 100 μm/1500 μm; (6) deposition of a 35 nm passivation film by ALD. Seven different passivating films were examined in this study: AHO, Al_2O_3, HfO_2, ZrO_2, TiO_2 deposited with two different chemistries, and TiO_2(3 nm)/Al_2O_3(2 nm) nanolaminate (TAO). For the highly flexible devices shown in Figure S6, the thicknesses of the channel and passivation layer were reduced to 9 and 20 nm, respectively, to enhance the devices' mechanical flexibility. Details of the ALD dielectric, channel, and passivation processes are provided below.

2.2. Atomic Layer Deposition. A Savannah 100 ALD system by Cambridge Nanotech Inc. was used to deposit the dielectric (AHO), ZnO channel, and passivation layer. The ALD chamber pressure was 0.1 Torr during the process with a constant 20 sccm flow of N_2 throughout to carry and purge the precursor vapors. The process conditions of the dielectric, channel, and passivation layers are summarized in Table 1. The metal−organic precursors used in the ALD processes included trimethylaluminum (TMA) (Sigma-Aldrich, 97% purity, used as received), tetrakis(dimethylamido) hafnium (TDMAHf) (Sigma-Aldrich, ≥99.99% purity, used as received), diethylzinc (DEZn) (Sigma-Aldrich, 97% purity, used as received), tetrakis(dimethylamido) zirconium (TDMAZr) (Sigma-Aldrich, ≥99.99% purity, used as received), tetrakis(dimethylamido) titanium (TDMATi) (Sigma-Aldrich, ≥99.99% purity, used as received), and titanium isopropoxide (TTIP) (Sigma-Aldrich, ≥99.99% purity, used as received). A 0.5 nm (5 cycles) Al_2O_3 layer was used as the initial nucleation layer for the AHO dielectric, whose process parameters were as follows: 0.1 s pulse of TMA, 30 s soak, 30 s purge, 0.1 s pulse of H_2O, 30 s soak, 30 s purge.

2.3. Characterization. The $I-V$ characteristics of the ZnO TFTs were measured in air with a Keithley 4200-SCS semiconductor characterization system with the gate voltages scanned from −2 to +10 V and the transfer curves taken at a drain bias of +8 V (in the saturation regime). Carrier concentration of the ZnO channel was measured with a HMS-3000 Hall-effect measurement system operated at room temperature. Water vapor transmission rates (WVTR) were measured with a permeation tester (MOCON AQUATRAN model 1) with 10 cm^2 samples at 38−60 °C and 90% relative humidity according to ISO 15106-3; the samples for WVTR measurements were prepared by depositing ALD barrier films on PET substrates. In the case where the WVTR of a sample at 38 °C was below the detection limit of the permeation tester (5×10^{-4} g m^{-1} day^{-1}), elevated-temperature measurements (up to 60 °C) were conducted to determine the activation energy for permeation, which was then substituted into the Arrhenius equation to extrapolate the 38 °C WVTR value of that sample. X-ray photoelectron spetroscopy (XPS) analyses were carried out in a XPS spectrometer (ULVAC-PHI 5000 VersaProbe) with a monochromatic Al Kα X-ray source (1486.6 eV); samples were cleaned by in situ Ar-sputtering (removing 1−3 nm of thickness) before measurement. X-ray diffraction (XRD) analyses were carried out in a Rigaku TTRAX 3 XRD system with a copper Kα line source.

2.4. Bias-Stress and Storage Tests. Bias-stress test was conducted by applying a constant +8 V bias-stress on the gate electrode of the tested TFTs in air and measuring the electrical characteristics of the TFTs at various times. Similarly, storage test was conducted by storing the tested TFTs in the ambient air (28 °C with 60% relative humidity) and measuring the electrical characteristics of the TFTs at various times.

3. RESULTS AND DISCUSSION

3.1. Characteristics and Stability of ALD ZnO TFTs without Passivation. The ZnO TFTs were fabricated with an ALD Al_2O_3/HfO_2 dielectric and an ALD ZnO channel layer (see Figure 1 for a schematic illustration of the device structure) to facilitate their subsequent integration with an ALD passivation process. The characteristics of the ALD ZnO TFTs without passivation were determined as references for our following analysis on the effects of passivation, and the results are shown in Figure 1 and Table 2. The TFTs exhibited

Table 2. Characteristics of ZnO TFTs with and without a Passivation Layer: Field-Effect Mobility (μ), Subthreshold Swing (SS), Threshold Voltage (V_{th}), and On/Off Ratio

	μ (cm^2 V^{-1} s^{-1})	SS (V $decade^{-1}$)	V_{th} (V)	on/off ratio
no passivation	16.6 ± 0.5	0.42 ± 0.04	2.4 ± 0.2	1×10^5
TiO_2- or TAO-passivated	20.2 ± 0.4	0.38 ± 0.02	2.4 ± 0.17	1×10^5

excellent device characteristics, with field-effect mobility ~17 cm^2 V^{-1} s^{-1} and subthreshold swing (SS) ~ 0.4 V $decade^{-1}$. This was especially remarkable considering that the processing temperature was much lower (90 °C for both the dielectric and channel layers) than what is typical in TFT fabrication, and that the process did not require a postdeposition annealing step, which was a standard procedure in typical TFT fabrication. In fact, this was the first time in our knowledge that such high device performance was achieved at such low processing temperature. As a point of reference, previous works using similarly low processing temperatures to fabricate ZnO TFTs achieved much lower field-effect mobility at 1−12 $cm^2/(V\ s)$ and larger SS at 0.5−0.7 V $decade^{-1}$.[25,29,40] The high device performance was attributed to the high quality of the low-temperature-processed ALD films and their interfaces. It should be noted that in order to magnify the effects of passivation for better analysis of the underlying mechanism, the ZnO channel layer was not patterned (i.e., it covered the entire substrate surface). As a result, the off current and gate leakage current (see Supporting Information, Figure S1) of the devices were relatively high, even though the gate dielectric was of high quality, with a low leakage current density of 10^{-7} A cm^{-2} at <10 V and an estimated breakdown field of ~9 MV cm^{-1} (see Supporting Information, Figure S2).

The stability of the ALD ZnO TFTs were evaluated with two types of tests: a bias-stress test, where a constant +8 V gate voltage was applied to the TFTs in the ambient air, and a storage test, where the TFTs were stored without operation in the ambient air for a prolonged duration. The results of the stability tests are shown in Figures 2 and 3. In the bias-stress test, the threshold voltage (V_{th}) of the TFTs exhibited a

DOI: 10.1021/acsami.5b07278
ACS Appl. Mater. Interfaces 2015, 7, 22610−22617

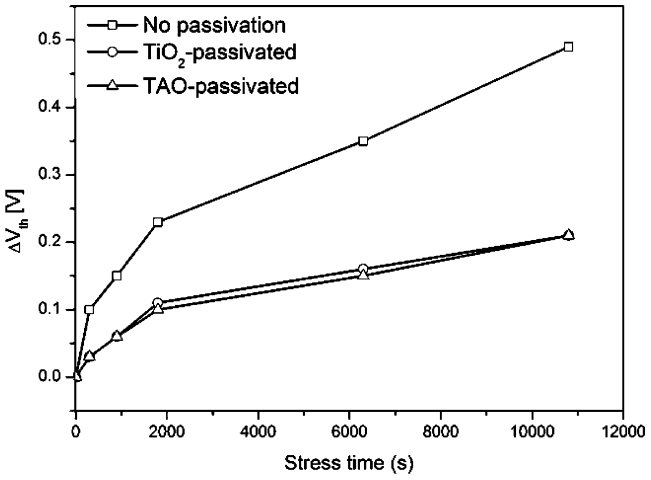

Figure 2. Change in the V_{th} (ΔV_{th}) of ZnO TFTs with/without passivation during the bias-stress test (constant +8 V gate bias).

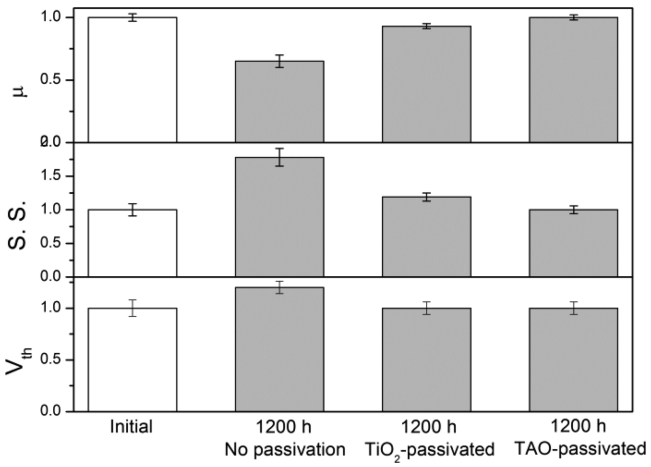

Figure 3. Changes in the field-effect mobility (μ), subthreshold swing (SS), and threshold voltage (V_{th}) of the ZnO TFTs during the storage test. The values shown are normalized against the initial μ, SS, and V_{th} values at the start of the test; the original data are included in Supporting Information, Table S3. The error bars were calculated from the results of 30 devices.

positive shift of 0.5 V after 10 800 s of stressing (Figure 2); the other device characteristics including on/off currents, mobility, and SS remained unchanged (see Supporting Information, Table S1). In the storage test (Figure 3), on the other hand, all of the device characteristics degraded significantly: V_{th} shifted by +0.5 V, mobility reduced by 40%, and SS nearly doubled after 1200 h of storage. The shifts in V_{th} in both tests were caused by diffusion of oxygen into the ZnO channel, from which the oxygen accepted electrons, thereby lowering the electron concentration.[41] The reduced mobility and raised SS in the storage test were due to incursion of moisture, which created charge-trapping defects in the channel and the channel/dielectric interface during operation.[42] The fact that only the effect of oxygen (V_{th} shift) was observed in the bias-stress test, even though the tested devices were also exposed to moisture in air, was because the applied bias prevented moisture from adsorbing to the channel layer.[2]

3.2. Passivation-Induced Degradations to ZnO TFTs. An ALD nanolaminated Al_2O_3/HfO_2 (AHO) film that we previously developed for encapsulating organic light-emitting diodes and solar cells[43] was initially used as the passivating layer for the ZnO TFTs. The AHO film at 35 nm thickness had an exceptionally low WVTR of 1×10^{-6} g m^{-2} day^{-1}, and therefore was expected to be capable of shielding the TFTs from any environment-induced degradation. However, upon deposition of the AHO film onto the ZnO TFTs, significant device degradations occurred, as shown in Figure 4. The AHO

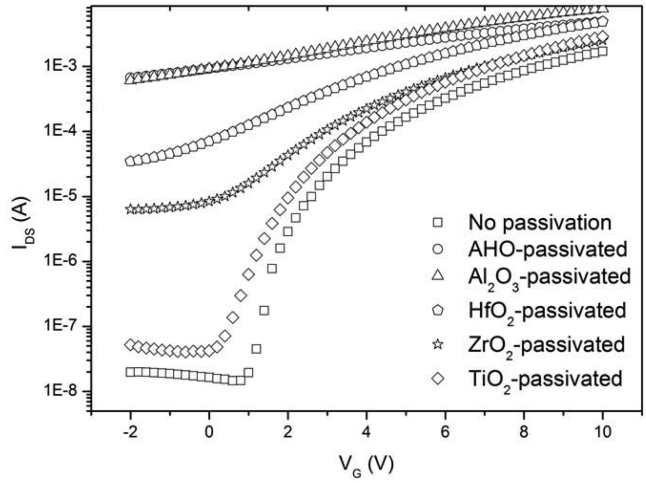

Figure 4. Transfer characteristics of the ZnO TFTs before and after being passivated with various ALD films.

passivating film caused the on- and off-currents to drastically increase and the V_{th} to shift to a negative value. These changes indicated an increase in the electron concentration in the ZnO channel, which was confirmed by Hall-effect measurements, where we found that the electron concentration increased from 4.2×10^{17} to 2.8×10^{18} cm^{-3} upon the application of the AHO film.

Similar passivation-induced degradations have previously been observed on ALD Al_2O_3-passivated ZnO-based TFTs, and the mechanism of the degradations has been identified as follows:[44,45] during the ALD passivation process, the metal–organic precursor of the ALD Al_2O_3 passivating film, trimethylaluminum (TMA), comes into contact with the ZnO channel, from which it extracts oxygen, leaving behind oxygen vacancies and increasing the electron concentration. Such oxygen extraction reaction has also been found to occur between other ALD metal–organic precursors and oxide semiconductors.[46]

3.3. Factors Determining Passivation-Induced Degradations. Given that the cause of ALD-passivation-induced degradations is extraction of oxygen from the oxide channel by the ALD metal–organic precursor, it stands to reason that using a precursor with weaker oxygen-extraction reactivity would reduce the magnitude of the degradations. Since the oxygen-extraction reaction involves a metal–organic precursor breaking its metal–ligand bonds to form metal–oxygen bonds, the oxygen-extraction tendency of the precursor may be quantified in terms of the difference between the bond energies, ΔBE, as given by

$$\Delta BE = BE_{M-O} - BE_{M-L} \quad (1)$$

where BE_{M-O} and BE_{M-L} are the bond energies of the metal–oxygen and the metal–ligand bonds, respectively.

To verify this reasoning, we examined the degradations to ZnO TFTs induced by four ALD passivating process, each of

DOI: 10.1021/acsami.5b07278
ACS Appl. Mater. Interfaces 2015, 7, 22610–22617

which used water and a metal−organic compound with a distinct ΔBE value as precursors. The metal−organic precursors in the order of decreasing ΔBE were TMA (for depositing Al_2O_3), tetrakis(dimethylamido) hafnium (TDMAHf) (for HfO_2), tetrakis(dimethylamido) zirconium (TDMAZr) (for ZrO_2), and tetrakis(dimethylamido) titanium (TDMATi) (for TiO_2). The ΔBE values were calculated from literature bond energy data and are summarized in Table 3. The

Table 3. ΔBE Values of TMA, TDMAZr, TDMAHf, and TDMATi and the Hall-Effect Electron Concentration of a ZnO Film Passivated with an ALD Process Employing Each of the Those Four Precursors[a]

precursor for passivation	ΔBE (kJ mol^{-1})	electron concentration of ZnO (cm^{-3})
No passivation	n/a	4.2×10^{17}
TMA (Al_2O_3)	314	2.8×10^{18}
TDMAZr (ZrO_2)	257	1.0×10^{18}
TDMAHf (HfO_2)	209	1.4×10^{18}
TDMATi (TiO_2)	164	5.1×10^{17}

[a]Bond energy data for calculating the ΔBE values are included in Supporting Information, Table S4.

TFT characteristics after passivation by these four films are shown in Figure 4, and the effects of the passivation films on the electron concentration of the ZnO channel were determined by Hall-effect measurements, as shown in Table 3. In agreement with our assumption, the magnitude of passivation-induced degradation as well as the increase in electron concentration indeed followed the same trend as that of the ΔBE, that is, TMA (Al_2O_3) > TDMAHf (HfO_2) > TDMAZr (ZrO_2) > TDMATi (TiO_2).

In addition to the intrinsic reactivity of precursors, the temperature of the passivation process was also a degradation-determining factor. Figure 5 presents the characteristics of ZnO TFTs before and after being passivated with a HfO_2 passivating film (using TDMAHf and H_2O) deposited at 90 or 150 °C. The 150 °C process caused greater increases in the off and on currents and a larger shift in the V_{th} than did the 90 °C deposited film. Similar temperature-dependency was also observed for the other types of films (see Supporting Information, Figure S4). The temperature-dependency was consistent with the reactivity-driven mechanism; that is, a higher processing temperature enhances the reactivity of a precursor, allowing it to more strongly extract oxygen from the ZnO channel.

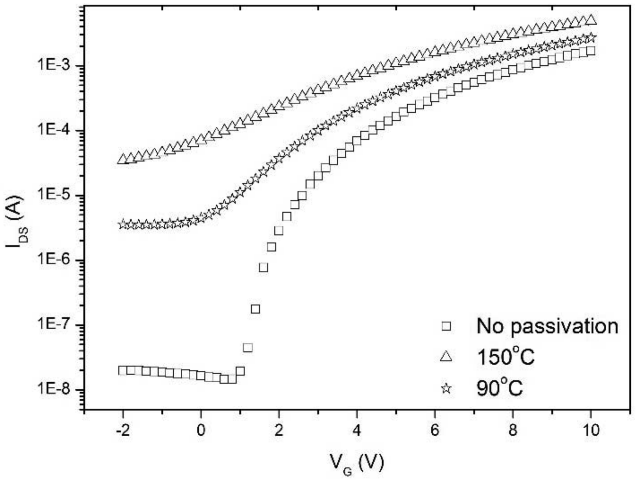

Figure 5. Effects of the passivation processing temperature on the transfer characteristics of ZnO TFTs passivated with a HfO_2 passivation layer (using TDMAHf and H_2O).

3.4. Eliminating Passivation-Induced Degradations. Having identified the degradation-determining factors, we designed the following ALD passivation process to eliminate passivation-induced degradations on ZnO TFTs. We selected a metal−organic precursor with minimum ΔBE, and operated at the low end of the process window of the ALD process. The precursor we selected was titanium isopropoxide (TTIP), whose metal−ligand bond is that of Ti−O and therefore has a nominally zero ΔBE. The ALD process was carried out at 110 °C. The resultant TiO_2 films were amorphous, as determined by X-ray diffraction (XRD) (see Supporting Information, Figure S5), and were nearly stoichiometric with negligible amount of carbon residue, as determined by X-ray photoelectron spectroscopy (XPS) (see Supporting Information, Table S2). The TiO_2 films were also reasonably good gas barrier, with a WVTR of 3×10^{-3} g m^{-2} day^{-1} at 38 °C (at 35 nm thickness).

Figure 6 and Table 2 present the characteristics of ZnO TFTs before and after being passivated with the TTIP/H_2O

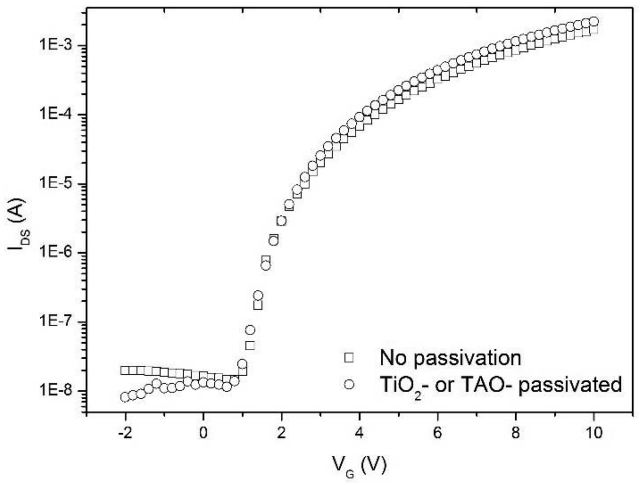

Figure 6. Transfer characteristics of ZnO TFTs before and after passivation with the TTIP/H_2O TiO_2 or the TAO process. Note that because the characteristics of the TiO_2- and TAO-passivated devices were identical, only one curve is shown to avoid confusion. A plot showing both TiO_2- and TAO-passivated curves is provided in Supporting Information, Figure S3.

ALD process. The TFTs indeed exhibited no observable change in the off-current and V_{th} after the encapsulation process, even with the unpatterned channel layer magnifying any damaging effect of passivation, as explained earlier. This was remarkable in that the TFTs did not require a high-termperature annealing step to recover demages incurred by the passivation process, which is a standard practice in TFT production.[47] Moreover, the TTIP/H_2O ALD process significantly improved the field-effect mobility and SS of the TFTs: mobility increased from 16.6 to 20.2 cm^2 V^{-1} s^{-1} and SS reduced from 0.42 to 0.38 V decade^{-1}. These improvements in TFT performance were attributed to removal of charge-trapping defects, for example, adsorded water molecules, from

DOI: 10.1021/acsami.5b07278
ACS Appl. Mater. Interfaces 2015, 7, 22610−22617

the surface of the ZnO channel layer via reactions with TTIP during the initial stage of the ALD passivation process.[42]

We also discovered that after a ZnO TFT was passivated with 3 nm of TiO_2 film utilizing the TTIP/H_2O process, when the TFT was then subjected to the TMA/H_2O Al_2O_3 process (which we showed earlier to be highly damaging), it did not exhibit any degradation. This indicated that the 3 nm TiO_2 film was sufficient to seal the ZnO channel from exposure to the high-reactivity TMA. In other words, the TTIP/H_2O process can be used as a pretreatment to allow subsequent ALD processes to be used, which may be necessary to improve upon the gas-barrier performance of the TiO_2 film. For example, we found that exceptional gas-barrier performance, WVTR < 10^{-6} g m^{-2} day^{-1} (see Supporting Information for measurement data), could be achieved with an alternating TiO_2(3 nm)/Al_2O_3(2 nm) nanolaminated (TAO) film (35 nm of total thickness). Using the TAO film to passivate ZnO TFTs, with the TTIP/H_2O TiO_2 process applied first, also resulted in degradation-free passivation, as shown in Figure 5 and Table 2.

3.5. Stability of ALD-Passivated Flexible ZnO TFTs. Stability of the ZnO TFTs passivated with the TiO_2 or the TAO film were evaluated with the bias-stress and storage tests described earlier, and the results are shown in Figures 2 and 3. Compared with the results from the without-passivation devices, the TiO_2- or TAO-passivated TFTs showed remarkable improvements in both bias-stress and storage stability. In the bias-stress test (Figure 2), the V_{th} of the TiO_2- or TAO-passivated TFTs shifted by only < +0.2 V after 10 800 s of bias-stressing, down from ∼+0.5 V of the without-passivation device. Despite the much lower gas permeability of TAO film than that of the TiO_2 film (WVTR < 1×10^{-6} vs 3×10^{-3} g m^{-2} day^{-1}), the changes in V_{th} during the bias-stress test were the same for the TiO_2 and the TAO-passivated devices. This indicated that the small observed Vth shifts of the passivated devices were due to intrinsic defects instead of environment-induced ones.[48]

In the storage test, on the other hand, where the time scale was much larger than that of the bias-stress test, the difference between the TiO_2 and the TAO-passivated devices became discernible, although both showed significant improvements over the without-passivation devices (Figure 3). The TAO passivation film, with its lower gas permeability, obtained better storage stability: the mobility and SS remained unchanged after 1200 h of storage in air. It should be noted that since the ZnO TFTs were on PET substrates, which were poor gas barriers with a WVTR of 0.3 g m^{-2} day^{-1}, an additional gas barrier was also required to prevent air from entering the devices through the substrates (see Figure 1 for a schematic illustration). This function was conveniently provided by the ALD AHO dielectric layer, which as mentioned earlier had a low WVTR of ∼10^{-6} g m^{-2} day^{-1}.[49] The excellent stability of the ZnO TFTs indicated that the combination of the ALD TAO passivating layer and the ALD AHO dielectric layer successfully eliminated environment-induced degradations to the TFTs.

In terms of mechanical flexibility of the PET-based TFT devices, thanks to the small thicknesses of the ALD dielectric, channel, and passivation layers, the devices were able to withstand a reasonably high degree of bending: the device characteristics remained constant after repeated bending (up to 1000 times) at 1.3 cm of radius of curvature, as shown in Supporting Information (Figure S6). The gas-barrier performance of the TAO passivation and the AHO dielectric layers were unaffected by the bending as well, as the TFT devices showed the same stability before and after bending, that is, the same < +0.2 V shift in V_{th} after extended bias-stressing. To improve beyond the current degree of flexibility, ALD organic–inorganic hybrid nanolaminated films[50] will likely have to be introduced into the TFT devices, which is the topic of our ongoing work.

4. CONCLUSIONS

Flexible plastics-based ZnO TFTs with excellent device characteristics and stability (field-effect mobility > 20 cm^2 V^{-1} s^{-1}, SS < 0.4 V $decade^{-1}$, nearly intact characteristics after bias-stressing for 10 800 s, air storage for 1200 h, and repeated bending to 1.3 cm radius) were fabricated with a low-temperature (≤110 °C) integrated ALD process which deposited the dielectric, channel, and passivation layers, minimizing defects at the interfaces. The severe problem of ALD-passivation-induced defects to ZnO TFTs was resolved by minimizing the oxygen-extraction tendency of the metal–organic precursor of the ALD passivation process. Specifically, degradation-free passivation of ZnO TFTs was demonstrated with an ALD TiO_2 process using TTIP as the metal–organic precursor and a low deposition temperature of 110 °C. In addition to avoiding ZnO TFT degradations, the TiO_2 film, when combined with an ALD Al_2O_3 film into TiO_2/Al_2O_3 nanolaminates, also provided exceptional gas-barrier performance, that is, WVTR < 1×10^{-6} g m^{-2} day^{-1}, which adequately insulated the TFTs from environment-induced degradation, resulting in the observed high stability. Our results demonstrated for the first time the fabrication of stable and high-performance flexible ZnO TFTs without requiring a high deposition temperature or a high-temperature annealing step, which will greatly enhance the manufacturability of ZnO and other oxide-based TFTs.

■ ASSOCIATED CONTENT

Supporting Information

The Supporting Information is available free of charge on the ACS Publications website at DOI: 10.1021/acsami.5b07278.

Details of WVTR measurements; gate leakage currents and leakage current density of the dielectric layer; additional device characteristics as a function of passivation condition; XRD and XPS results; device characteristics of flexible TFTs after bending; bond energy data used to calculate the DBE values in Table 3 (PDF)

■ AUTHOR INFORMATION

Corresponding Author

*E-mail: ftsai@ntu.edu.tw.

Notes

The authors declare no competing financial interest.

■ ACKNOWLEDGMENTS

This work was supported by Ministry of Science and Technology (Grant Nos. 103-2221-E-002-278, 103-2623-E-002-003-ET, 102-2221-E-002-231, 102-3113-E-007-001), Industrial Technology Research Institute, and Bureau of Energy, Ministry of Economic Affairs of Taiwan. The authors thank Prof. Miin-Jang Chen of Institute of Materials Science and Engineering at National Taiwan University for providing device characterization equipment.

DOI: 10.1021/acsami.5b07278
ACS Appl. Mater. Interfaces 2015, 7, 22610–22617

REFERENCES

(1) Kamiya, T.; Nomura, K.; Hosono, H. Present Status of Amorphous In−Ga−Zn−O Thin-Film Transistors. *Sci. Technol. Adv. Mater.* **2010**, *11*, 044305.

(2) Jeong, J. K.; Yang, H. W.; Jeong, J. H.; Mo, Y.-G.; Kim, H. D. Origin of Threshold Voltage Instability in Indium-Gallium-Zinc Oxide Thin Film Transistors. *Appl. Phys. Lett.* **2008**, *93*, 123508.

(3) Fakhri, M.; Theisen, M.; Behrendt, A.; Goerrn, P.; Riedl, T. Top-Gate Zinc Tin Oxide Thin-Film Transistors with High Bias and Environmental Stress Stability. *Appl. Phys. Lett.* **2014**, *104*, 251603.

(4) Fakhri, M.; Johann, H.; Goerrn, P.; Riedl, T. Water as Origin of Hysteresis in Zinc Tin Oxide Thin-Film Transistors. *ACS Appl. Mater. Interfaces* **2012**, *4*, 4453−4456.

(5) Fakhri, M.; Goerrn, P.; Weimann, T.; Hinze, P.; Riedl, T. Enhanced Stability against Bias-Stress of Metal-Oxide Thin Film Transistors Deposited at Elevated Temperatures. *Appl. Phys. Lett.* **2011**, *99*, 123503.

(6) Illiberi, A.; Scherpenborg, R.; Theelen, M.; Poodt, P.; Roozeboom, F. On the Environmental Stability of ZnO Thin Films by Spatial Atomic Layer Deposition. *J. Vac. Sci. Technol., A* **2013**, *31*, 061504.

(7) Görrn, P.; Riedl, T.; Kowalsky, W. Encapsulation of Zinc Tin Oxide Based Thin Film Transistors. *J. Phys. Chem. C* **2009**, *113*, 11126−11130.

(8) Fakhri, M.; Babin, N.; Behrendt, A.; Jakob, T.; Görrn, P.; Riedl, T. Facile Encapsulation of Oxide Based Thin Film Transistors by Atomic Layer Deposition Based on Ozone. *Adv. Mater.* **2013**, *25*, 2821−2825.

(9) Carcia, P. F.; McLean, R. S.; Groner, M. D.; Dameron, A. A.; George, S. M. Gas Diffusion Ultrabarriers on Polymer Substrates Using Al_2O_3 Atomic Layer Deposition and SiN Plasma-Enhanced Chemical Vapor Deposition. *J. Appl. Phys.* **2009**, *106*, 023533.

(10) Carcia, P. F.; McLean, R. S.; Reilly, M. H. High-Performance ZnO Thin-Film Transistors on Gate Dielectrics Grown by Atomic Layer Deposition. *Appl. Phys. Lett.* **2006**, *88*, 123509.

(11) Heo, J.; Hock, A. S.; Gordon, R. G. Low Temperature Atomic Layer Deposition of Tin Oxide. *Chem. Mater.* **2010**, *22*, 4964−4973.

(12) Meyer, J.; Görrn, P.; Bertram, F.; Hamwi, S.; Winkler, T.; Johannes, H.-H.; Weimann, T.; Hinze, P.; Riedl, T.; Kowalsky, W. Al_2O_3/ZrO_2 Nanolaminates as Ultrahigh Gas-Diffusion Barriers—A Strategy for Reliable Encapsulation of Organic Electronics. *Adv. Mater.* **2009**, *21*, 1845−1849.

(13) Dameron, A. A.; Davidson, S. D.; Burton, B. B.; Carcia, P. F.; McLean, R. S.; George, S. M. Gas Diffusion Barriers on Polymers Using Multilayers Fabricated by Al_2O_3 and Rapid SiO_2 Atomic Layer Deposition. *J. Phys. Chem. C* **2008**, *112*, 4573−4580.

(14) Carcia, P. F.; McLean, R. S.; Sauer, B. B.; Reilly, M. H. Atomic Layer Deposition Ultra-Barriers for Electronic Applications-Strategies and Implementation. *J. Nanosci. Nanotechnol.* **2011**, *11*, 7994−7998.

(15) Ritala, M.; Kalsi, P.; Riihela, D.; Kukli, K.; Leskela, M.; Jokinen, J. Controlled Growth of TaN, Ta_3N_5, and TaO_xN_y Thin Films by Atomic Layer Deposition. *Chem. Mater.* **1999**, *11*, 1712−1718.

(16) Miikkulainen, V.; Leskela, M.; Ritala, M.; Puurunen, R. L. Crystallinity of Inorganic Films Grown by Atomic Layer Deposition: Overview and General Trends. *J. Appl. Phys.* **2013**, *113*, 021301.

(17) Leskela, M.; Ritala, M. Atomic Layer Deposition Chemistry: Recent Developments and Future Challenges. *Angew. Chem., Int. Ed.* **2003**, *42*, 5548−5554.

(18) Leskela, M.; Ritala, M. Atomic Layer Deposition (ALD): From Precursors to Thin Film Structures. *Thin Solid Films* **2002**, *409*, 138−146.

(19) Hamalainen, J.; Ritala, M.; Leskela, M. Atomic Layer Deposition of Noble Metals and Their Oxides. *Chem. Mater.* **2014**, *26*, 786−801.

(20) Alen, P.; Vehkamaki, M.; Ritala, M.; Leskela, M. Diffusion Barrier Properties of Atomic Layer Deposited Ultrathin Ta_2O_5 and TiO_2 Films. *J. Electrochem. Soc.* **2006**, *153*, G304−G308.

(21) Poodt, P.; Lankhorst, A.; Roozeboom, F.; Spee, K.; Maas, D.; Vermeer, A. High-Speed Spatial Atomic-Layer Deposition of Aluminum Oxide Layers for Solar Cell Passivation. *Adv. Mater.* **2010**, *22*, 3564−3567.

(22) Poodt, P.; Knaapen, R.; Illiberi, A.; Roozeboom, F.; van Asten, A. Low Temperature and Roll-to-Roll Spatial Atomic Layer Deposition for Flexible Electronics. *J. Vac. Sci. Technol., A* **2012**, *30*, 01A142.

(23) Vermang, B.; Rothschild, A.; Racz, A.; John, J.; Poortmans, J.; Mertens, R.; Poodt, P.; Tiba, V.; Roozeboom, F. Spatially Separated Atomic Layer Deposition of Al_2O_3, a New Option for High-Throughput Si Solar Cell Passivation. *Prog. Photovoltaics* **2011**, *19*, 733−739.

(24) Hoye, R. L. Z.; Munoz-Rojas, D.; Nelson, S. F.; Illiberi, A.; Poodt, P.; Roozeboom, F.; MacManus-Driscoll, J. L. Research Update: Atmospheric Pressure Spatial Atomic Layer Deposition of ZnO Thin Films: Reactors, Doping, and Devices. *APL Mater.* **2015**, *3*, 040701.

(25) Illiberi, A.; Cobb, B.; Sharma, A.; Grehl, T.; Brongersma, H.; Roozeboom, F.; Gelinck, G.; Poodt, P. Spatial Atmospheric Atomic Layer Deposition of $In_xGa_yZn_zO$ for Thin Film Transistors. *ACS Appl. Mater. Interfaces* **2015**, *7*, 3671−3675.

(26) Illiberi, A.; Poodt, P.; Bolt, P.-J.; Roozeboom, F. Recent Advances in Atmospheric Vapor-Phase Deposition of Transparent and Conductive Zinc Oxide. *Chem. Vap. Deposition* **2014**, *20*, 234−242.

(27) Illiberi, A.; Scherpenborg, R.; Roozeboom, F.; Poodt, P. Atmospheric Spatial Atomic Layer Deposition of In-Doped ZnO. *ECS J. Solid State Sci. Technol.* **2014**, *3*, P111−P114.

(28) Yanguas-Gil, A.; Elam, J. W. Analytic Expressions for Atomic Layer Deposition: Coverage, Throughput, and Materials Utilization in Cross-Flow, Particle Coating, and Spatial Atomic Layer Deposition. *J. Vac. Sci. Technol., A* **2014**, *32*, 031504.

(29) Levy, D. H.; Freeman, D.; Nelson, S. F.; Cowdery-Corvan, P. J.; Irving, L. M. Stable ZnO Thin Film Transistors by Fast Open Air Atomic Layer Deposition. *Appl. Phys. Lett.* **2008**, *92*, 192101.

(30) Heo, J.; Kim, S. B.; Gordon, R. G. Atomic Layer Deposited Zinc Tin Oxide Channel for Amorphous Oxide Thin Film Transistors. *Appl. Phys. Lett.* **2012**, *101*, 113507.

(31) Wang, X.; Saadat, O. I.; Xi, B.; Lou, X.; Molnar, R. J.; Palacios, T.; Gordon, R. G. Atomic Layer Deposition of Sc_2O_3 for Passivating AlGaN/GaN High Electron Mobility Transistor Devices. *Appl. Phys. Lett.* **2012**, *101*, 232109.

(32) Zhang, X.-H.; Kippelen, B. High-Performance C-60 N-Channel Organic Field-Effect Transistors through Optimization of Interfaces. *J. Appl. Phys.* **2008**, *104*, 104504.

(33) Zhang, X.-H.; Domercq, B.; Wang, X.; Yoo, S.; Kondo, T.; Wang, Z. L.; Kippelen, B. High-Performance Pentacene Field-Effect Transistors Using Al_2O_3 Gate Dielectrics Prepared by Atomic Layer Deposition (ALD). *Org. Electron.* **2007**, *8*, 718−726.

(34) Zhang, X.-H.; Lee, S. M.; Domercq, B.; Kippelen, B. Transparent Organic Field-Effect Transistors with Polymeric Source and Drain Electrodes Fabricated by Inkjet Printing. *Appl. Phys. Lett.* **2008**, *92*, 243307.

(35) Zhang, M.-H.; Tiwari, S. P.; Kippelen, B. Pentacene Organic Field-Effect Transistors with Polymeric Dielectric Interfaces: Performance and Stability. *Org. Electron.* **2009**, *10*, 1133−1140.

(36) Tiwari, S. P.; Zhang, X.-H.; Potscavage, W. J.; Kippelen, B. Low-Voltage Solution-Processed N-Channel Organic Field-Effect Transistors with High-K HfO_2 Gate Dielectrics Grown by Atomic Layer Deposition. *Appl. Phys. Lett.* **2009**, *95*, 223303.

(37) Kim, J. B.; Fuentes-Hernandez, C.; Hwang, D. K.; Potscavage, W. J., Jr.; Cheun, H.; Kippelen, B. Vertically Stacked Hybrid Organic-Inorganic Complementary Inverters with Low Operating Voltage on Flexible Substrates. *Org. Electron.* **2011**, *12*, 45−50.

(38) Jun, T.; Yoshihiro, U.; Koji, Y.; Mami, F.; Yasuaki, I.; Yukiharu, U.; Kazushige, T.; Hiroshi, T. Comparison between Effects of PECVD-SiOx and Thermal ALD-AlOx Passivation Layers on Characteristics of Amorphous InGaZnO TFTs. *ECS J. Solid State Sci. Technol.* **2015**, *4*, 61−65.

(39) Jun, T.; Song, K.; Jung, Y.; Jeong, S.; Moon, J. Bias Stress Stable Aqueous Solution Derived Y-doped ZnO Thin Film Transistors. *J. Mater. Chem.* **2011**, *21*, 13524−13529.

DOI: 10.1021/acsami.5b07278
ACS Appl. Mater. Interfaces 2015, 7, 22610−22617

(40) Oh, B. Y.; Kim, Y. H.; Lee, H. J.; Kim, B. Y.; Park, H. G.; Han, J. W.; Heo, G. S.; Kim, T. W.; Kim, K. Y.; Seo, D. S. High-Performance ZnO Thin-Film Transistor Fabricated by Atomic Layer Deposition. *Semicond. Sci. Technol.* **2011**, *26*, 085007.
(41) Kang, Y.-J.; Kim, C. S.; Kwack, W.-S.; Ryu, S. Y.; Song, M.; Kim, D.-H.; Hong, S. W.; Jo, S.; Kwon, S.-H.; Kang, J.-W. Amorphous Gallium Indium Zinc Oxide Thin Film Transistors: Sensitive to Oxygen Molecules. *Appl. Phys. Lett.* **2007**, *90*, 192101.
(42) Park, J.-S.; Jeong, J. K.; Chung, H.-J.; Mo, Y.-G.; Kim, H. D. Electronic Transport Properties of Amorphous Indium-Gallium-Zinc Oxide Semiconductor upon Exposure to Water. *Appl. Phys. Lett.* **2008**, *92*, 072104.
(43) Chang, C.-Y.; Chou, C.-T.; Lee, Y.-J.; Chen, M.-J.; Tsai, F.-Y. Thin-Film Encapsulation of Polymer-Based Bulk-Heterojunction Photovoltaic Cells by Atomic Layer Deposition. *Org. Electron.* **2009**, *10*, 1300−1306.
(44) Na, J.-S.; Peng, Q.; Scarel, G.; Parsons, G. N. Role of Gas Doping Sequence in Surface Reactions and Dopant Incorporation during Atomic Layer Deposition of Al-Doped ZnO. *Chem. Mater.* **2009**, *21*, 5585−5593.
(45) Elam, J. W.; George, S. M. Growth of ZnO/Al_2O_3 Alloy Films Using Atomic Layer Deposition Techniques. *Chem. Mater.* **2003**, *15*, 1020−1028.
(46) Lee, S. W.; Lee, Y. S.; Heo, J.; Siah, S. C.; Chua, D.; Brandt, R. E.; Kim, S. B.; Mailoa, J. P.; Buonassisi, T.; Gordon, R. G. Improved Cu2O-Based Solar Cells Using Atomic Layer Deposition to Control the Cu Oxidation State at the P-N Junction. *Adv. Energy Mater.* **2014**, *4*, 1301916.
(47) Nomura, K.; Kamiya, T.; Ohta, H.; Hirano, M.; Hosono, H. Defect Passivation and Homogenization of Amorphous Oxide Thin-Film Transistor by Wet O_2 Annealing. *Appl. Phys. Lett.* **2008**, *93*, 192107.
(48) Lee, J.-M.; Cho, I.-T.; Lee, J.-H.; Kwon, H.-I. Bias-Stress-Induced Stretched-Exponential Time Dependence of Threshold Voltage Shift in InGaZnO Thin Film Transistors. *Appl. Phys. Lett.* **2008**, *93*, 093504.
(49) Chang, C.-Y.; Tsai, F.-Y. Efficient and Air-Stable Plastics-Based Polymer Solar Cells Enabled by Atomic Layer Deposition. *J. Mater. Chem.* **2011**, *21*, 5710−5715.
(50) Vähä-Nissi, M.; Pitkänen, M.; Salo, E.; Kenttä, E.; Tanskanen, A.; Sajavaara, T.; Putkonen, M.; Sievänen, J.; Sneck, A.; Rättö, M. Antibacterial and Barrier Properties of Oriented Polymer Films with ZnO Thin Films Applied with Atomic Layer Deposition at Low Temperatures. *Thin Solid Films* **2014**, *562*, 331−337.

DOI: 10.1021/acsami.5b07278
ACS Appl. Mater. Interfaces 2015, 7, 22610−22617